### Title

Heteroaggregation of CeO2 and TiO2 engineered nanoparticles in the aqueous phase: Application of turbiscan stability index and fluorescence excitation-emission matrix (EEM) spectra




### Authors

Luo, Muxi
Qi, Xuejiao
Ren, Tongxuan
et al.



### Publication Date

2017-11-01

### DOI

10.1016/j.colsurfa.2017.08.014

Peer reviewed

Colloids and Surfaces A 533 (2017) 9–19

Contents lists available at ScienceDirect

Colloids and Surfaces A

journal homepage: www.elsevier.com/locate/colsurfa

# Heteroaggregation of $CeO_2$ and $TiO_2$ engineered nanoparticles in the aqueous phase: Application of turbiscan stability index and fluorescence excitation-emission matrix (EEM) spectra

Muxi Luo[a,1], Xuejiao Qi[a,1], Tongxuan Ren[a], Yuxiong Huang[b], Arturo A. Keller[b], Hongtao Wang[a,*], Boran Wu[a], Huapeng Jin[a], Fengting Li[a]

[a] State Key Laboratory of Pollution Control and Resource Reuse, Key Laboratory of Yangtze River Water Environment, Ministry of Education, College of Environmental Science and Engineering, Tongji University, Shanghai 200092, China
[b] Bren School of Environmental Science and Management, University of California, Santa Barbara, CA, 93106, United States

## GRAPHICAL ABSTRACT

The utilization of TSI and Fluorescence EEM spectra can overcome the limitation of traditional methods and tools for heteroaggregation.

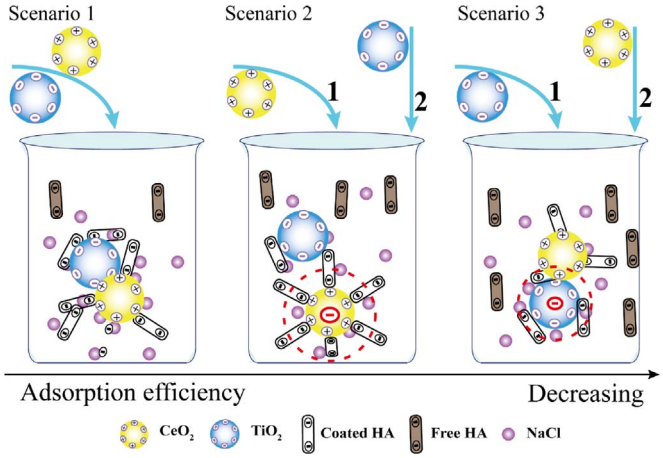


## ARTICLE INFO

*Keywords:*
Heteroaggregation
Turbiscan stability index
Cerium oxide nanoparticles
Titanium dioxide nanoparticles
Fluorescence EEM spectra

## ABSTRACT

$CeO_2$ and $TiO_2$ engineered nanoparticles (ENPs) are being increasingly used in many applications. Due to their properties, heteroaggregation between these two types of ENPs is very likely, which can determine their fate and transport. However, the heteroaggregation behavior of $CeO_2$ and $TiO_2$ ENPs is still not clear, partly due to the lack of appropriate tools. In this study, we investigated the application of Turbiscan Stability Index (TSI) for the measurements of $CeO_2$/$TiO_2$ ENP heteroaggregation. TSI was found to be effective to investigate the heteroaggregation and stability of the $CeO_2$-$TiO_2$ ENPs system. Increasing $CeO_2$/$TiO_2$ ENPs ratio reduces the TSI values, indicating higher stability. Fluorescence excitation-emission matrix (EEM) spectra were used to study the interface interaction between humic acid (HA) and $CeO_2$/$TiO_2$ ENPs. The TSI value of ENPs were rising with the increasing of $CeO_2$/$TiO_2$ ENPs ratios in the H River or Q Reservoir water. In addition, their variation trends were

* Corresponding author.
*E-mail addresses:* hongtao@tongji.edu.cn, wanght010@gmail.com (H. Wang).
[1] These authors contributed equally to this work as first authors.

http://dx.doi.org/10.1016/j.colsurfa.2017.08.014
Received 6 June 2017; Received in revised form 12 August 2017; Accepted 12 August 2017
Available online 18 August 2017
0927-7757/ 

similar to those in well-controlled synthetic water. Proposed interaction mechanisms include surface charge attraction and competitive adsorption.

## 1. Introduction

Engineered nanoparticles (ENPs) are being increasingly used in commercial products [1,2]. As a result, significant amounts of ENPs (e.g. nano-$CeO_2$, nano-$TiO_2$, nano-Ag, nano-ZnO, $C_{60}$ and et al.) may be released into natural systems, potentially affecting human and ecological health [3,4]. Therefore, many studies have addressed the transport and fate of ENPs, which can be used to estimate predicted exposure concentrations [4–7]. However, most studies have focused on homoaggregation and transport [8–10] or heteroaggregation between ENPs and natural colloids (NCs) [11–13], while very few studies have addressed the heteroaggregation between two types of ENPs in synthetic [14] and natural waters [15]. In addition, using mixtures of several ENPs in pollution control [16,17] or medicine [18,19] has become more common, which makes it more important to study the heteroaggregation of different ENPs.

$CeO_2$ and $TiO_2$ ENPs are extensively used in industry and environmental research including admixed photoelectrodes for natural dye-sensitized solar cells [20], photocatalysts [21], counter electrode for electrochromic devices [22] and herbicides [23]. Karunakaran et al. found that the surface properties and synthesis behavior among $CeO_2$ and $TiO_2$ ENPs affect their aggregation behavior [24]. In addition, studies demonstrated that the aggregation process influences the photoelectric effect of ENPs [7,25]. Therefore, there is a need to study the heteroaggregation between $CeO_2$ and $TiO_2$ ENPs.

Most heteroaggregation studies have used dynamic light scattering (DLS) and attachment efficiency for understanding these processes [14,26,27]. Dusak et al. suggested that the mass ratios of multiwall carbon nanotubes (MCNTs) and hematite nanoparticles (Hem ENPs) (15 g/L) have influence on the heteroaggregation rates as measured by DLS and their zeta potential [28]. DLS can be applied in both homo- and heteroaggregation experiments, however, only changes of particle size can be measured [29]. If we apply the approaches designed for homoaggregation to study heteroaggregation, the results will be concentration dependent, which must be taken into consideration [29]. Thus, find an appropriate way to describe the stability and heteroaggreation behavior of nanoparticles would be one of the key question in the study of heteroaggreation.

The turbiscan stability index (TSI) requires no sample dilution and can be utilized for a wide range of concentrations and particle sizes [30]. The basic principle is to measure both transmittance and backscatter of infrared light at different wavelengths; the stability of the system can be evaluated from the scan [31]. TSI has been applied to study the stability of emulsions [31–33] and the coagulation properties of goat's milk [34] as well as the stability and heteroaggregation behavior of alumina-silica oxide ENPs (hydrodynamic diameter 112 nm–496 nm, 1 g/L) suspension [35,36]. In detail, TSI was used to study the changes of the stability of the emulsions treated by different homogenization rates [31]. For studying the effects of ultrasound pretreatment on the stability of the goat milk, TSI was calculated based on backscattering changes, and was used to evaluate the degree of particle aggregation [37]. To investigate the effects of polymers on the stability of the aluminum oxide and alumina-silica, TSI was also used to measure the changes of the stability in the presence and absence of the polymer and polyacrylic acid, respectively [38,39]. Therefore, TSI may be applied to characterize the heteroaggregation behavior and stability of $CeO_2$ and $TiO_2$ ENPs mixtures. Compared with ultraviolet-visible spectrophotometry and DLS, TSI can be used to measure binary systems and extremely unstable systems. Ultraviolet-visible spectrophotometry is usually used to analyze homoaggregation of samples with characteristic peaks, such as nano-Ag, nano-ZnO, nano-Cu and nano-$CeO_2$ [40–44]. TSI is influenced by particle size and volume concentration of the system, and is also appropriate for measuring extreme unstable system compared with DLS, which can only reflect the changes of the particle size [45–48].

In addition, natural organic matter (NOM) can influence the stability and aggregation of ENPs ($TiO_2$, $CeO_2$ and ZnO, 10 mg/L) [49,50]. Particularly, NOM can adsorb onto the surface of $TiO_2$ and $CeO_2$ ENPs, form a coating layer, result in steric hinderance and electrostatic repulsion and have effect on the heteroaggregation of ENPs [8,26,51]. Luo et al. [52] showed that the properties of humic acid (HA) and fulvic acid (FA) influence the adsorption and aggregation of $TiO_2$ ENPs (10 mg/L), indicating that NOM can adsorb onto the surface of $TiO_2$ ENPs. However, total organic carbon (TOC) measurements may not adequately characterize the aggregation behavior between ENPs at low NOM concentration [53]. Fluorescence excitation-emission matrix (EEM) can be combined with regional integration analysis to characterize the composition and transformation of humic and fulvic acids [54]. Fluorescence EEM has also been used to evaluate the aggregation of gold nanoparticles and humic substances by examining the quenching and enhancement of fluorescence [53]. Chen et al. used regional integration of fluorescence EEM to characterize the spectra of dissolved organic matter [55]. It is feasible to use fluorescence EEM spectra to analyze the adsorption of HA, which may influence the heteroaggregation of $CeO_2$ and $TiO_2$ ENPs.

In this study, different ratios of ENPs ($CeO_2$ and $TiO_2$) were used in heteroaggregation experiments, and the competitive adsorption of NOM by ENPs was investigated by changing the additive order of $CeO_2$ and $TiO_2$ ENPs. In addition, even though the total concentration of $TiO_2$ and $CeO_2$ ENPs (10 mg/L) is higher than that of natural situation and their behavior may be different, natural water samples were employed to study the heteroaggregation. A major goal was to explore the application of turbiscan stability index for the measurements of heteroaggregation between different NPs.

## 2. Materials and methods

### 2.1. $CeO_2$ and $TiO_2$ ENPs

$CeO_2$ and $TiO_2$ (anatase, P25) ENPs were purchased from Aladdin and Sigma-Aldrich, respectively. The primary morphologies and sizes of $CeO_2$ or $TiO_2$ ENPs were characterized by Transmission Electron Microscopy (TEM) (Fig. S1). Brunauer–Emmett–Teller (BET) surface area of $CeO_2$ and $TiO_2$ ENPs were determined by $N_2$ adsorption (Micromeritics ASAP2020), as listed in Table 1. A Malvern Zetasizer (Nano ZS 90, UK) was used to obtain the average hydrodynamic diameter and zeta potential (ξ) of $CeO_2$ or $TiO_2$ ENPs (Table 1). $CeO_2$ or $TiO_2$ ENPs stock suspensions (0.4 g/L) were prepared in Millipore water (Millipore, 18.2 MΩ·cm, TOC < 2 ppb). Fresh stocks were ultrasonicated for 20 min [56] and prepared daily. Isoelectric points of $CeO_2$ and $TiO_2$ are shown in Fig. S2.

### 2.2. Synthetic water

HA (Sigma-Aldrich (Shanghai) Trading Co., Ltd.) stock solutions were prepared by adding 16 mg HA into 100 mL Millipore water and then adjusting pH to 11 using 0.01 mol/L and 0.1 mol/L NaOH. The solution was stirred for 24 h to ensure complete dissolution and then centrifuged 6 min at 8000 rpm. Following centrifugation, the pH was adjusted to 7 and filtered using a 0.45 μm filter membrane. The stock

**Table 1**
Characterization of $CeO_2$ and $TiO_2$ ENPs.

| ENPs | Primary particle size[a] | BET Surface Area ($m^2/g$) | Hydrodynamic diameter (nm) | Zeta potential (mV)[b] | pH[c] | Isoelectric point[c] |
|---|---|---|---|---|---|---|
| $CeO_2$ | < 25 nm | 47.97 ± 2.94 | 60 ± 5 | 6.15 ± 0.32 | 6.78 | 6.80 |
| $TiO_2$ | < 25 nm | 49.35 ± 1.18 | 100 ± 3 | −25.32 ± 0.44 | 6.62 | 4.90 |

[a] As reported by the manufacturer.
[b] Zeta potential- pH = 8, $C_x$ = 10 mg/L.
[c] pH/Isoelectric point- $C_x$ = 10 mg/L.

was stored at 4 °C. To study the effect of low concentration HA for heteroaggregation of ENPs [52], HA = 1 mg/L, the TOC of the HA was 0.41 mg/L, as determined by Shimadzu TOC V-CPN.

Ionic strength (IS) was adjusted to 5 mmol/L NaCl solution (580 ± 5 μs/cm) which is close to the IS of many natural waters. Buffer was made up with borax and solution (2 mL 0.05 mol/L and 8 mL 0.2 mol/L, respectively) and used to adjust pH to 7.8 to simulate natural water pH (30 μL buffer) [57]. Our preliminary study showed that buffer IS did not influence the results.

### 2.3. Natural water

Usually, ENP aggregation behavior and stability varies in different natural waters [49]. In addition to the well-defined synthetic waters discussed above, two different natural waters were used: Qingcaosha Reservoir (Q Reservoir, Chongming County, Shanghai, China) and Huangpu River (H River, Shanghai, China). The water samples were filtered with a 0.45 μm filter membrane and then stored at 4 °C for further studies. These waters were characterized in terms of pH, IS, TOC and inductively coupled plasma-optic emission spectroscopy (ICP-OES), as shown in Table 2. Electric conductivity (E.C) was used to illustrate IS range.

### 2.4. Batch experiments

#### 2.4.1. Aggregation and co-sedimentation experiments

In these studies, 40 mg/L $CeO_2$ or $TiO_2$ ENPs stock suspensions were prepared by adding 10 mg $CeO_2$ or $TiO_2$ ENPs respectively into 250 mL Millipore water. To detect the dominant effect of $CeO_2$ and $TiO_2$ ENPs on heteroaggregation, the experiments were conducted by mixing $CeO_2$ and $TiO_2$ ENPs stock solution with different mass ratios (0.1/9.9, 1/9, 5/5, 9/1, 9.9/0.1), for a total concentration of 10 mg/L (Our preliminary study showed [26,52,58] that 10 mg/L ENPs could more clearly indicate the aggregation behavior even if it may be unable to represent low environment concentration of ENPs like ng/L or μg/L). 5 mmol/L NaCl was used to provide IS. Mixing was done via ultrasonication. Buffer was added into distilled water to adjust pH at 8, and then the stock solution was added. The test was performed under ultrasonic dispersion. The aggregation and stability of system was determined by Turbiscan (Formulaction, France). The co-sedimentation of the ENPs-NOM was measured by ICP.

**Table 2**
Properties of Q Reservoir water and H River water.

| | Q Reservoir water | H River water |
|---|---|---|
| pH | 7.73 ± 0.05 | 7.78 ± 0.05 |
| TOC (mg/L) | 1.10 ± 0.05 | 3.14 ± 0.05 |
| E.C (μs/cm) | 252 ± 5 | 517 ± 5 |
| $Al^{3+}$ (mg/L) | 0.11 | 0.20 |
| $Ca^{2+}$ (mg/L) | 17.14 | 16.99 |
| $K^{+}$ (mg/L) | 1.75 | 6.18 |
| $Mg^{2+}$ (mg/L) | 5.59 | 8.55 |
| $Na^{+}$ (mg/L) | 5.19 | 27.8 |

#### 2.4.2. Adsorption of HA on $CeO_2$ and $TiO_2$ ENPs

$CeO_2$ or $TiO_2$ ENPs (100 mg) were added into 250 mL Millipore water to achieve a 400 mg/L stock solution. To analyze the effect of NOM adsorption onto $CeO_2$ and $TiO_2$ ENPs, the experiments were conducted with different ENP ratios as described in Section 2.4.1. To study the adsorption effect of HA onto the surface of $CeO_2$ and $TiO_2$ NPs, the total concentration after mixing $CeO_2$ and $TiO_2$ ENPs suspensions at different ratios was 100 mg/L. HA stock solution (1 mg/L) was added to the system. IS was provided by 5 mmol/L NaCl. Borax buffer was employed by all experiments to stabilize pH at 7.8. The centrifuge tubes were shaken for 48 h under 25 °C at 150 rpm, followed by 6 min centrifugation at 8000 rpm. Filtration was conducted using a 20 mL syringe and 0.45 μm filter membrane.

The competitive adsorption of HA onto the surface of $CeO_2$ and $TiO_2$ ENPs was carried out in the same solution composition and external conditions as stated in Section 2.4.1. The addition order of $CeO_2$ or $TiO_2$ ENPs was changed. The centrifuge tubes were shaken for 24 h under 25 °C at 150 rpm. After that another ENP was injected into the solution slowly against the wall of the centrifuge tubes by pipettes, followed by a prolonged 24 h shaking for centrifugation (8000 rpm, 6 min) and filtration (0.45 μm).

### 2.5. Analysis

#### 2.5.1. Three-dimensional fluorescence EEM spectroscopy

A Luminescence spectrometer (FluoroMax-4, HORIBA Jobin Yvon Co., France) was used to measure the three-dimensional EEM spectra of HA which remained in the system after filtering. Excitation and emission wave-lengths were collected incrementally from 240 nm to 550 nm and from 250 nm to 550 nm at 5 nm steps, respectively. The slit widths for both excitation and emission were 5 nm and the scanning speed was kept at 4800 nm/min. To eliminate second-order Raleigh light scattering, a 290-nm emission cutoff filter was used during scanning. The fluorescence spectra of Millipore water were also measured to subtract water Raman scattering and background noise.

#### 2.5.2. Turbiscan tower for aggregation analysis

Turbiscan Tower (Formulaction, France) was used to qualitatively analyze the heteroaggregation behavior of $CeO_2$ and $TiO_2$ ENPs at 25 °C by the measurement of their stability index. The samples were prepared in a 20 mL flat-bottomed glass cylindrical sample cell with a height of around 43 mm. The heteroaggregation of the ENPs was analyzed using the transmittance and back-scattering data, which were determined at an angle of 180° and 135° from the incident light respectively [35].

The basic principle of Turbiscan is to measure both transmittance and backscatter of near-infrared pulsed light (λ = 880 nm) from the bottom to the neck of a container containing the suspension [59,60]. The physical principle of Turbiscan is based on the Lambert-Beer theory, as shown in formula (1)–(2). For the same sample, T is only influenced by λ (formula 1), and λ is influenced by particle size (d) and volume concentration of dispersion phase (Ø). Therefore, T is influenced by d and Ø, and d is the major influence factor if the initial Ø is controlled [30].

$$T(\lambda, r_i) = T_0 e^{-\frac{2r_i}{\lambda}} \quad (1)$$

$$\lambda(d,\emptyset) = \frac{2d}{3\emptyset Q_s} \quad (2)$$

Where:

T: Transmittance value;

λ: Mean free-path of photon;

$r_i$: Vial inner radius;

d: The average particle size;

Ø: Volume concentration of dispersion phase;

$Q_s$: Optical Parameters according to Mie theory.

For backscattering, it is also affected by particle size and volume concentration of the sample with the suspension, as shown in formula (3).

$$BS = \sqrt{\frac{3\emptyset(1-g)Q_s}{2d}} \quad (3)$$

Where:

BS: Backscatter value;

Ø: Volume concentration of dispersion phase;

g: optical parameter based on Mie theory;

$Q_s/d$: The same with formula (1).

By such scanning (20 s/scan), the stability of the suspension can be evaluated by the uniformity of the light scattering at different depths with a wavelength of 880 nm [31]. TSI have been detected during the experiment and can be calculated as formula (4) [30]:

$$TSI = \sum_i \frac{\sum_h |Scan_i(h) - Scan_{i-1}(h)|}{H} \quad (4)$$

Where:

TSI: Turbiscan stability index.

H: Sample height from bottom of the cell to the meniscus.

$Scan_i(h)$: The $_i(h)$ scan at a given height h.

$Scan_{i-1}(h)$: The $_{i-1}(h)$ scan at a given height h.

i: as times from 1 to k (k = total time/scan speed).

The mean value of TSI changes with different particle stability states [32]. The TSI increases for larger particle sizes, indicating lower stability. In this study, the TSI of the middle zone (13.799 mm to 27.598 mm) of the sample cell was measured.

### 2.5.3. TEM

TEM (JEOL JEM-2011, operated at 200 kV) was employed to study the heteroaggregation states of HA-coated-$CeO_2$ and $TiO_2$ ENPs. The suspension samples were dropped upon the copper-grid-support and dried by infrared light.

## 3. Results and discussion

### 3.1. TSI measurements of heteroaggregation at different $CeO_2/TiO_2$ ENPs ratios

As shown in Fig. 1, TSI values decreased with increasing $CeO_2/TiO_2$

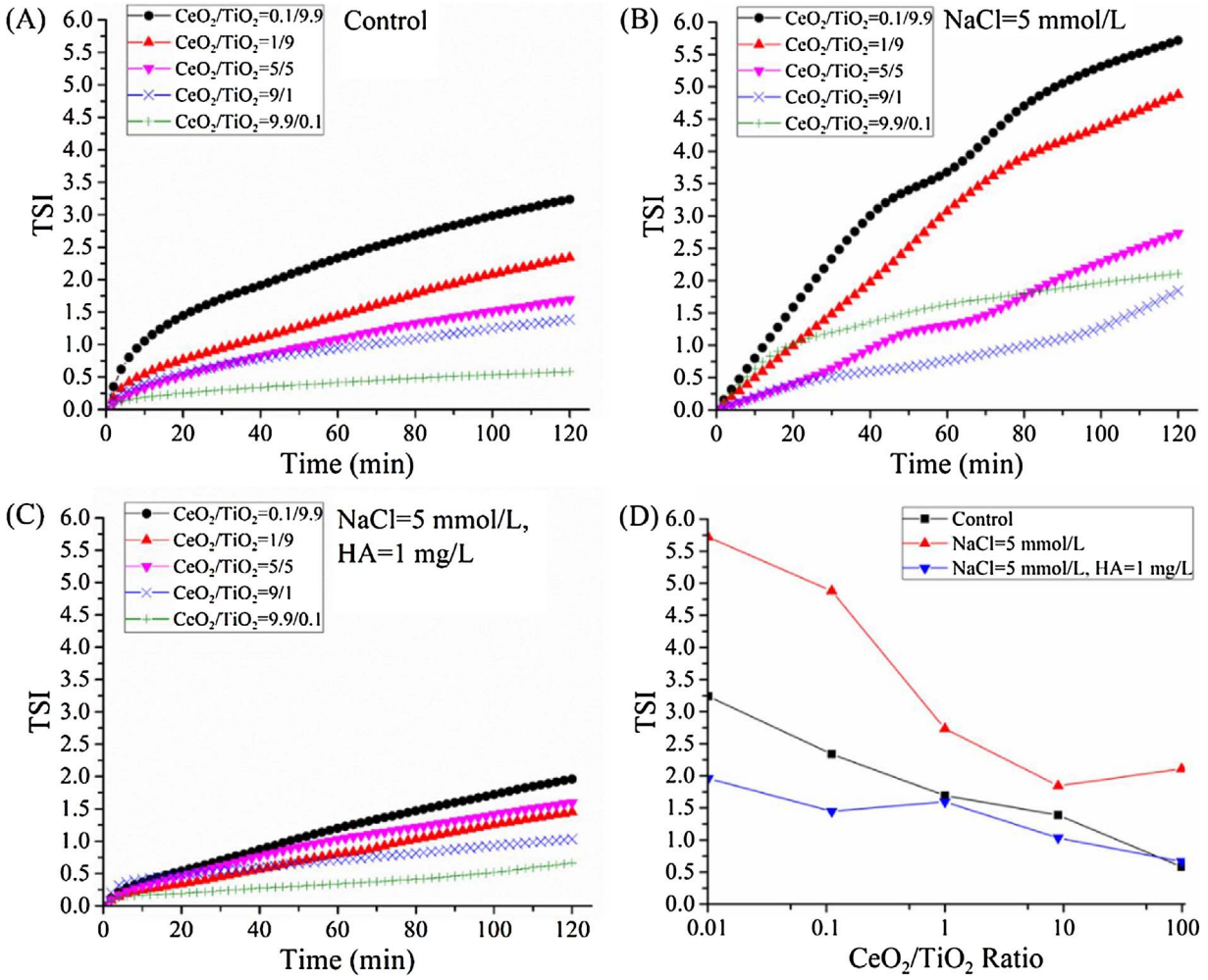


**Fig. 1.** TSI value of the system with different $CeO_2/TiO_2$ ENPs ratios: (A) Control; (B) NaCl = 5 mmol/L; (C) NaCl = 5 mmol/L, HA = 1 mg/L; (D) TSI of the system under different conditions after 2 h.

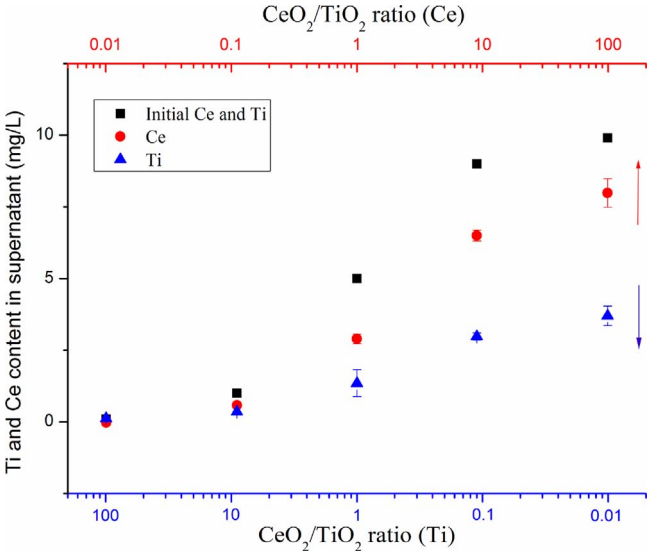


**Fig. 2.** Ce and Ti content in the supernatant at different $CeO_2/TiO_2$ ratios.

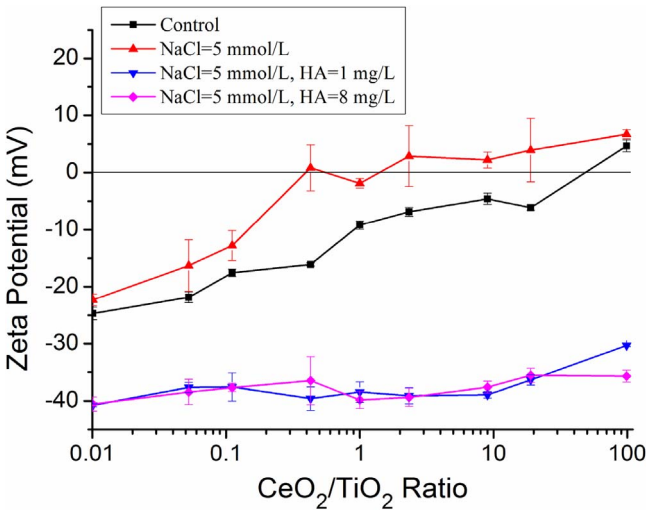


**Fig. 3.** Zeta potential of suspension under different $CeO_2/TiO_2$ ENPs ratios (pH = 7.8), $\xi_{TiO_2}$ = 6.15 mV and $\xi_{CeO_2}$ = -25.32 mV.

ENPs ratios, indicating higher stability. The addition of NaCl or HA influenced the TSI of the system (ENPs – HA – NaCl). NaCl was added to the system, TSI increased for specific $CeO_2/TiO_2$ ENPs ratios relative to no NaCl (Fig. 1(A) and (B)). These results indicate that IS will lead to the compression of the electric double layer and charge screening [52]. When both 5 mmol/L NaCl and 1 mg/L HA were added into the suspension (Fig. 1(C)), the TSI decreased significantly relative to the control and the 5 mmol/L NaCl. It is likely that HA was adsorbed on the surface of the ENPs and resulted in steric hindrance [8,61]. As a result, the addition of HA stabilized the system [52].

Fig. 2 shows the contents of Ti and Ce in the supernatant at different ratios. In the system, homoaggregation and heteroaggregation happened simultaneously[62]. It can be seen that the initial content of $TiO_2$ when the $CeO_2/TiO_2$ ratio varies from 100 to 0.01 is the same with the initial content of $CeO_2$ when $CeO_2/TiO_2$ ratio varies from 0.01 to 100. The content of $CeO_2$ in the supernatant is always higher than that of $TiO_2$ when the initial content of $CeO_2$ and $TiO_2$ are the same. The $TiO_2$ content ($CeO_2/TiO_2$ = 0.01) is higher than $CeO_2$ ($CeO_2/TiO_2$ = 100) in the supernatant. It seems homoaggregation of $TiO_2$ occurs more easily than that of $CeO_2$, and $TiO_2$ is easier to precipitate. Therefore, with a decreasing $TiO_2$ content, the TSI decreases and the stability of the system increases.

However, Fig. 1(B) shows that when $CeO_2/TiO_2$ = 9.9:0.1, TSI is higher than when $CeO_2/TiO_2$ = 9:1 and 5:5. This may be because when $CeO_2/TiO_2 \leq$ 9:1, NaCl contributes to the homoaggreagtion of $TiO_2$ or the heteroaggregation of $CeO_2$ and $TiO_2$. Therefore, with decreasing of $TiO_2$ content, TSI decreases. However, when $CeO_2/TiO_2$ = 9.9:0.1, $TiO_2$ content is very low, and NaCl will promote the homoaggregation of $CeO_2$, increasing the TSI and the decreasing of stability of the system.

As shown in Fig. 3, the surface charge of the ENPs in suspension changed from negative to positive with an increase in $CeO_2/TiO_2$ ENPs ratio, in the absence of HA and NaCl. When there was only $CeO_2$ or $TiO_2$ ENPs at an ENP concentration of 10 mg/L and pH 7.8, their zeta potential was 6.15 mV and −25.32 mV, respectively. The addition of NaCl (increasing IS) generally shifted the charge towards more positive. In a higher IS system, a $CeO_2/TiO_2$ ENPs ratio < 0.5 was needed to reverse the charge of the heteroaggregated particles; at that ratio they are essentially neutral and should be quite unstable. This may be attributed to IS compressing the electrical double layer and charge neutralization between $CeO_2$ and $TiO_2$ ENPs [63,64]. Therefore, IS will lead to destabilization of heteroaggregated $CeO_2$ and $TiO_2$ ENPs significantly, but it is a function of $CeO_2/TiO_2$ ENPs ratio.

Both high (8 mg/L) and low (1 mg/L) concentrations of HA resulted in a slight change of the surface charge of the ENPs with an increasing $CeO_2/TiO_2$ ENPs ratio. It is likely that HA adsorbed on the surface of ENPs and then restricted the contact between ENPs [65,66]. Therefore, HA increases the negative charges on the surface and stabilizes the $CeO_2/TiO_2$ ENPs system.

It should be noted that without HA and with an increasing $CeO_2/TiO_2$ ratio, TSI decreases (Fig. 1) and the stability of the system increases. However, the absolute value of the zeta potential is closer to 0 with an increasing of $CeO_2/TiO_2$ ratio. Because $TiO_2$ is more likely to homo- and heteroaggregation than $CeO_2$, the stability of the system increases with an increasing $CeO_2/TiO_2$ ratio. Since $\xi_{TiO_2}$ = 6.15 mV and $\xi_{CeO_2}$ = −25.32 mV, the zeta potential of the whole system increases and is closer to 0 with the increasing of $CeO_2/TiO_2$ ratio. However, the contact surface of $TiO_2$ and $CeO_2$ ENPs decreases because of the decreasing amount of $TiO_2$ ENPs. In addition, homoaggregation of $CeO_2$ is less likely. Therefore, although the zeta potential of the whole system was closer to 0, the stability of the system increased because of the limited contact surface of $CeO_2$ and $TiO_2$ and the poor ability of $CeO_2$ to homoaggregate.

### 3.2. Interaction of humic acid on the surface of $CeO_2$ and $TiO_2$ ENPs

Fluorescence was employed to qualitatively study the adsorption of HA onto $CeO_2/TiO_2$ ENPs, by analyzing peak location and fluorescence intensity. The three-dimensional EEM fluorescence spectra of HA (1 mg/L) at different $CeO_2/TiO_2$ ENPs ratios are presented in Fig. 4. Only one regional peak could be identified from the fluorescence spectra. The peak located at an excitation/emission (Ex/Em) wavelength of 240–245/415–425 nm, which is the characteristic fluorescence peak of HA. The peak intensity correlated positively with HA concentration [55,67]. Compared to the initial Ex/Em of 245/430 nm for HA with no ENPs present, the peak location showed a blue shift along both excitation and emission axes and the fluorescence peak intensity also decreased when ENPs were present (Table S1). This shift is related to a decrease in hydrophilic functional groups such as carbonyl, hydroxyl, amine and an elimination of π-electron systems [68]. Therefore, the blue shift of the fluorescence peak indicated that HA adsorbs via hydrophilic functional groups to the ENPs [53].

As shown in Fig. 4-scenario 1, the fluorescence intensity decreased with increasing $CeO_2/TiO_2$ ENPs ratio, which indicates a stronger adsorption of HA at higher $CeO_2/TiO_2$ ENPs ratios (Fig. S3). This is in accordance with the decrease in TSI values (Fig. 1) and increasing zeta potential (Fig. 3). These results indicate that HA may be more easily adsorbed on the surface of $CeO_2$ ENPs with an increasing $CeO_2/TiO_2$

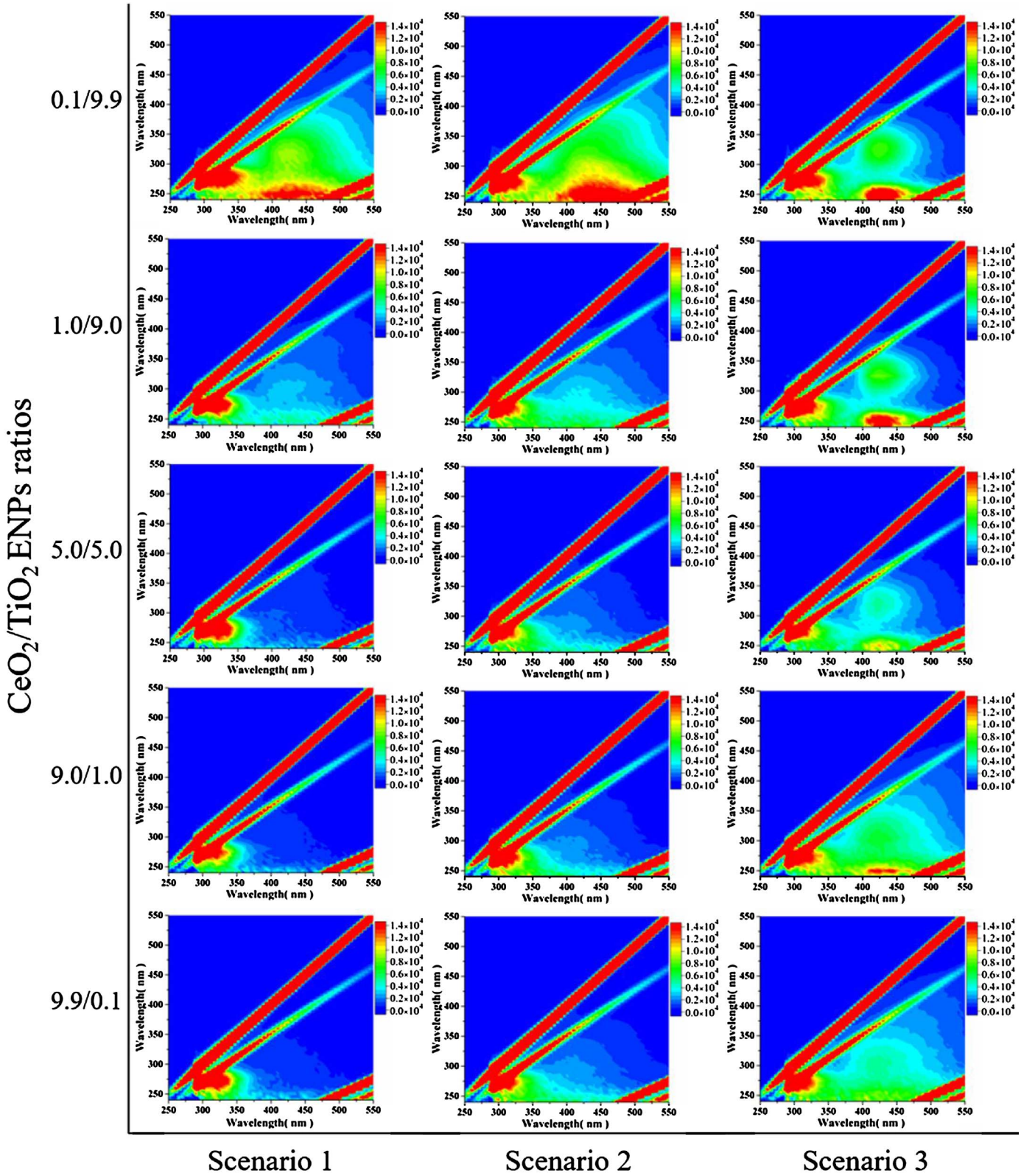


**Fig. 4.** Fluorescence EEM spectra of HA at different $CeO_2/TiO_2$ ENPs ratios: 0.1/9.9, 1/9, 5/5, 9/1, 9.9/0.1. Condition: NaCl = 5 mmol/L, HA = 1 mg/L, total concentration of $CeO_2$ and $TiO_2$ = 100 mg/L.

Note: Scenario 1: $CeO_2$ and $TiO_2$ ENPs simultaneously;

Scenario 2: $CeO_2$ first, $TiO_2$ ENPs later;

Scenario 3: $TiO_2$ first, $CeO_2$ ENPs later.

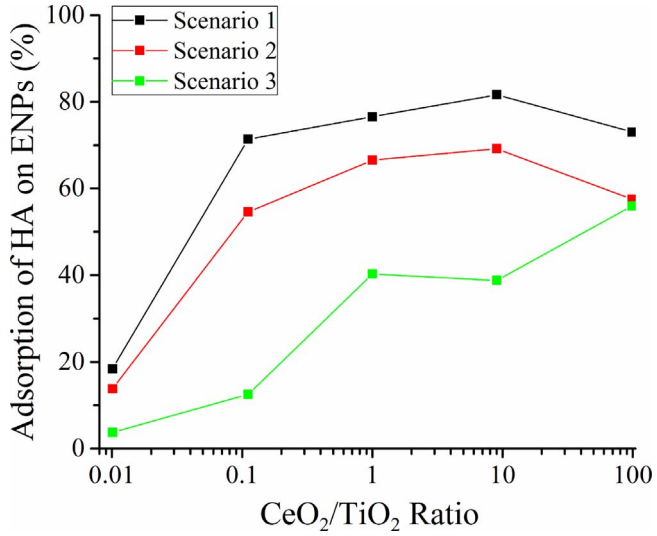


**Fig. 5.** Adsorption of HA on ENPs at different $CeO_2/TiO_2$ ENPs ratios. (Condition: NaCl = 5 mmol/L, HA = 1 mg/L, total concentration of $CeO_2$ and $TiO_2$ = 100 mg/L).

ENPs ratio. To study the competitive adsorption of HA to $CeO_2$ and $TiO_2$ ENPs, the addition ratio and order of ENPs were varied: scenario 1, $CeO_2$ and $TiO_2$ ENPs simultaneously; scenario 2, $CeO_2$ first, $TiO_2$ later; scenario 3, $TiO_2$ first, $CeO_2$ later. As shown in Fig. 4- scenario 2 and scenario 3, the fluorescence intensity decreased with increasing $CeO_2/TiO_2$ ENPs ratio, but varied with addition order. When the addition of $CeO_2$ and $TiO_2$ ENPs was simultaneous, the adsorption of HA on the surface of ENPs reached 81.6%, which is higher than the other sequences (scenario 1 and 2) (Fig. 5). The percentage adsorption of scenario 3 was significantly less than for scenario 2. This result indicates that increasing the $CeO_2/TiO_2$ ENPs ratio generally leads to the higher adsorption of HA, but the maximum adsorbed depends on the addition order.

We propose a mechanism of the competitive adsorption of HA by $CeO_2$ and $TiO_2$ ENPs (Fig. 6). When $CeO_2$ and $TiO_2$ ENPs are added to the system, they have opposite surface charges (Fig. 3), so that electrostatic attraction, including patch attraction, plays a major role, resulting in more aggregation[69]. Therefore, the $CeO_2/TiO_2$ ENPs heteroaggregate has a high HA adsorption capacity (Fig. 5). At scenario 2, the positively charged $CeO_2$ ENPs can adsorb HA and shift the heteroaggregate (HA on $CeO_2$ ENPs) to a negative surface charge (Fig. 3), before contacting $TiO_2$ ENPs. Further, the negatively charged $TiO_2$ ENPs will experience some electrostatic repulsion from $CeO_2$-HA, decreasing adsorption efficiency. However, at scenario 3, few HA are initially adsorbed onto the surface of $TiO_2$ ENPs. Once $CeO_2$ ENPs is added, it interacts with $TiO_2$-HA, which has higher electronegativity than $TiO_2$ ENPs and HA. As a result, the interaction of $CeO_2$-$TiO_2$-HA is less than that of $CeO_2$-HA, possibly due to adsorption competition [70]. This suggests that HA occupies some adsorption sites of these ENPs first and thus decreases the availability of "pristine" ENPs surface for further interactions [71]. HA functions as stabilizing agent by binding with nanoparticles and restricting the heteroaggregation [72].

### 3.3. Co-sedimentation of $CeO_2$ and $TiO_2$ ENPs under different ratios

Although turbidity has been used to characterize the aggregation and sedimentation of nanoparticles [8,58], it should be noted that turbidity is not appropriate to represent the sedimentation of $CeO_2/TiO_2$ ENPs due to the differences in intensity of scattered light. Therefore, Ti and Ce concentrations in the supernatant were determined using ICP after 2 h. As shown in Fig. 7, the Ce content is less than Ti in the supernatant (the top 2 mL in 20 mL tube) under the same conditions. In addition, HA markedly hindered the sedimentation of both $CeO_2$ and $TiO_2$ ENPs, as well as their heteroaggregate because of electrostatic repulsion [26,73].

As shown in Fig. 8, in the absence of HA, $CeO_2$ and $TiO_2$ ENPs experience heteroaggregation and destabilization due to electrostatic attraction. However, with increasing $CeO_2/TiO_2$ ENPs ratio, the homoaggregation of $CeO_2$ ENPs plays a major role [14,74]. $CeO_2$ ENPs homoaggregation results in a decreasing TSI, indicating the system is more stable. In the presence of HA, HA is adsorbed onto the surface of ENPs, with a strong preference for $CeO_2$ ENPs. This causes steric

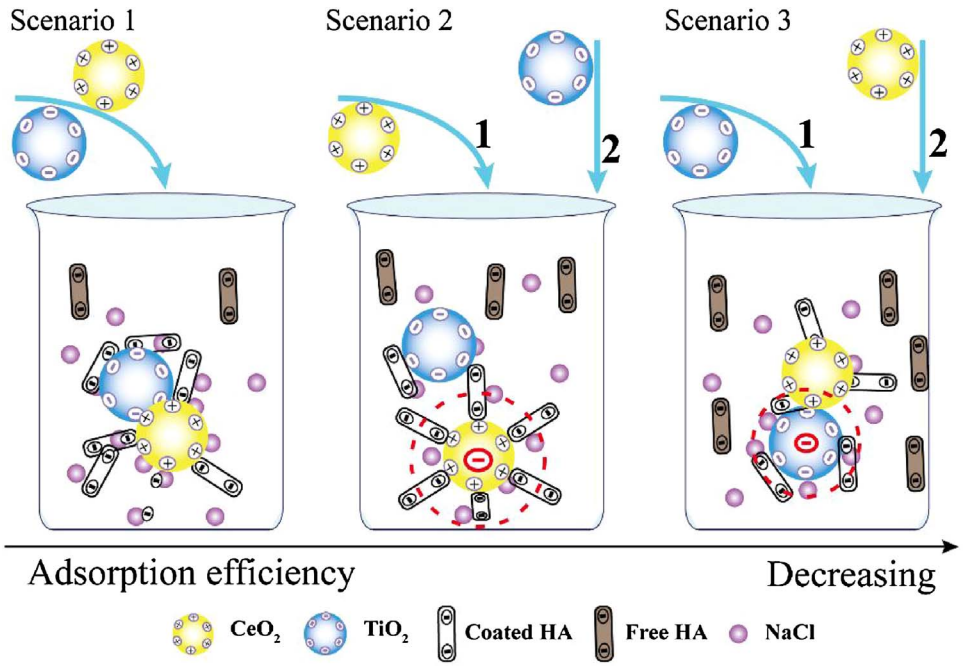


**Fig. 6.** Proposed mechanisms for the competitive adsorption of HA to $CeO_2$ and $TiO_2$ ENPs under hydrostatic condition, depending on the order of addition.

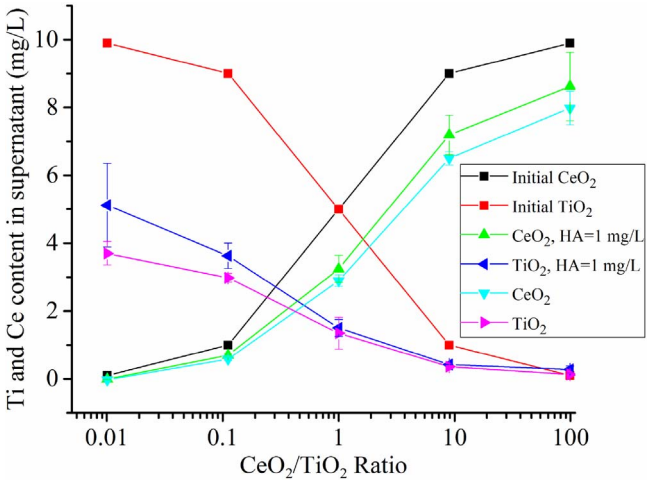


**Fig. 7.** The concentration of Ce or Ti in the supernatant under different $CeO_2/TiO_2$ ratios: 0.1/9.9, 1/9, 5/5, 9/1, 9.9/0.1. (Condition: NaCl = 5 mmol/L, total concentration of $CeO_2$ and $TiO_2$ = 10 mg/L, 2 h *Part of data is from Fig. 2).

hindrance between $CeO_2$ and $TiO_2$ ENPs and weakens their heteroaggregation. HA will reduce the TSI value and result in decreasing sedimentation [75]. Therefore, in the presence of HA aggregation and sedimentation of $CeO_2$ ENPs is less than that of $TiO_2$ ENPs.

### 3.4. Heteroaggregation of different $CeO_2/TiO_2$ ENPs ratios in natural water

Fig. 9 shows the change in TSI values with various $CeO_2/TiO_2$ ENPs ratios in natural water. When $TiO_2$ and $CeO_2$ ENPs were added into H River water, the TSI of the system decreased with increasing $CeO_2/TiO_2$ ENPs ratio (shown in Fig. 9(A)). At $CeO_2/TiO_2$ ENPs = 9.9/0.1, the TSI value changed slightly (only 0.72) in 2 h. In comparison, the variation became noticeable (2.91) at $CeO_2/TiO_2$ ENPs = 0.1/9.9. When $TiO_2$ and $CeO_2$ ENPs were added into Q Reservoir water (shown in Fig. 9(B)), the TSI variation showed similar trends. In addition, the TSI value variation trends of ENPs in the H River or Q Reservoir water were similar to those in well-controlled synthetic water.

The differences in TSI change between H River and Q Reservoir is very small (Fig. 9(C)). Interestingly, by testing the zeta potential of different $CeO_2/TiO_2$ ENPs ratios (Fig. 9(D)), we found these results were similar in H River or Q Reservoir waters. This result was inconsistent with previous studies which indicated that the zeta potential of system was different with NOM and IS [49,76]. As reported [12,37], the aggregation of ENPs may be limited by NOM and promoted by IS. It may be attributed to antagonism interaction of HA and IS on the heteroaggregation of $CeO_2$ and $TiO_2$ ENPs.

## 4. Conclusion

In this study, we successfully applied the turbiscan stability index (TSI) to characterize the heteroaggregation process of $CeO_2$ and $TiO_2$ ENPs. We believe it is an applicable approach for understanding and measuring heteroaggregation in general. TSI values decreased with increasing $CeO_2/TiO_2$ ENPs ratios, indicating the system became more stable and exhibited slower heteroaggregation. HA decreases the zeta potential of the system and strongly influences charge neutralization between the different surface charges of $CeO_2$ and $TiO_2$ ENPs. The three-dimensional EEM fluorescence spectra exhibited a blue shift in the presence of ENPs (Ex/Em of 245/430 nm), indicating that HA was adsorbed onto the surface of $CeO_2$ and $TiO_2$ ENPs. In addition, HA occupies some adsorption sites of these ENPs and the maximum adsorption depends on the addition order. From co- sedimentation experiments, we determined that the aggregation and sedimentation rate of $CeO_2$ ENPs was lower than for $TiO_2$ ENPs. Based on the Turbiscan and Fluorescence EEM spectra measurements, we proposed the interaction mechanisms of $CeO_2$ and $TiO_2$ ENPs heteroaggregation in the presence of HA, including surface charge attraction/repulsion and competitive adsorption.

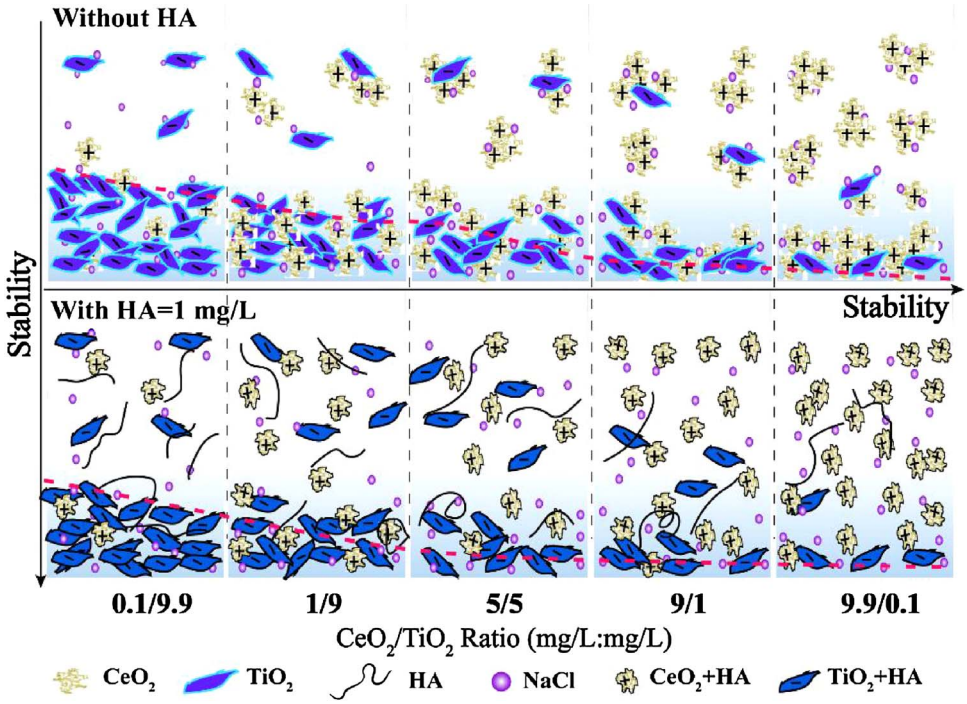


**Fig. 8.** Proposed heteroaggregation and sedimentation behaviors of $CeO_2$ and $TiO_2$ ENPs under different ratios.

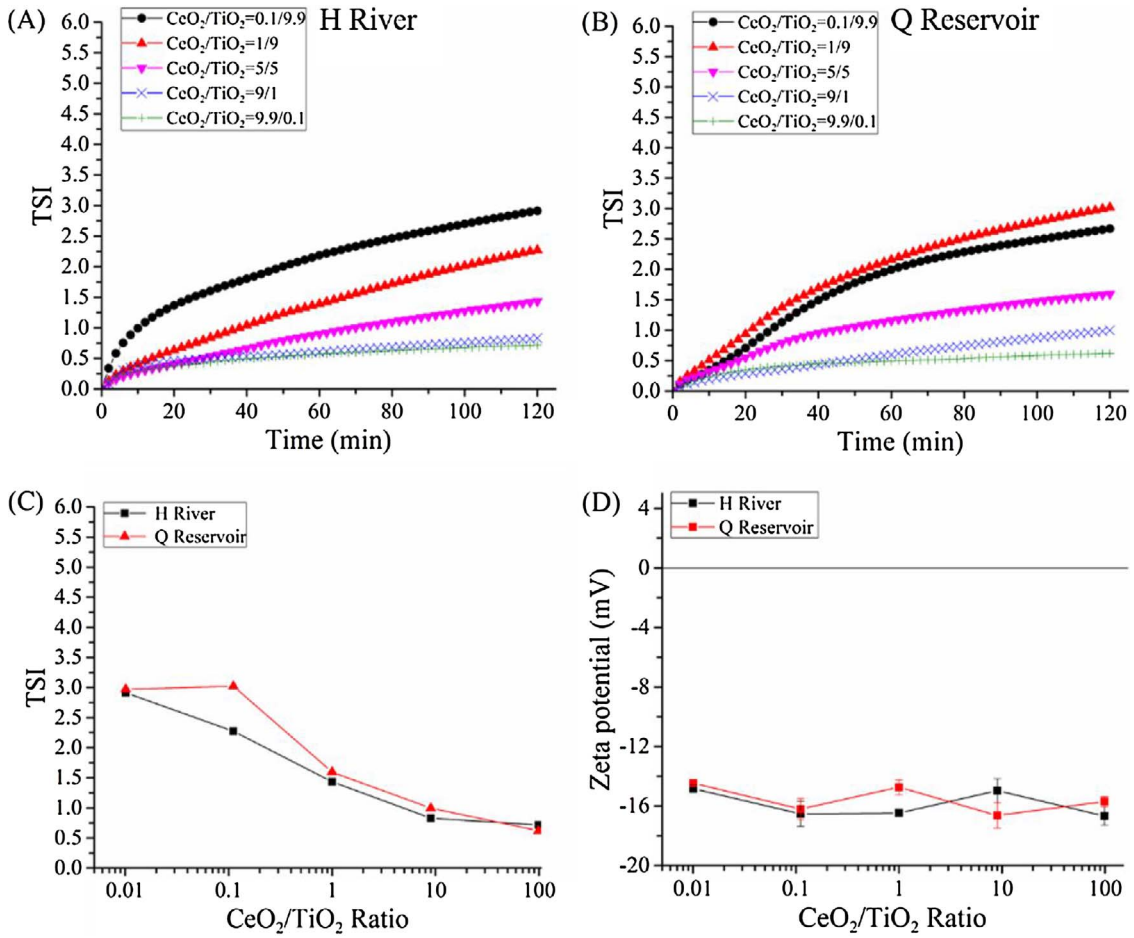


**Fig. 9.** TSI of different $CeO_2/TiO_2$ ENPs ratios in natural waters: (A) H River; (B) Q Reservoir; (C) TSI of the system after 2 h; (D) zeta potential of the system.


## Acknowledgments

The research was partially supported by special fund of State Key Joint Laboratory of Environment Simulation and Pollution Control (No. 16K07ESPCT), Science and Technology Commission of Shanghai Municipality (No. 15230724300), and National Natural Science Foundation of China Fund (No. 51108328). This work was also partially supported by the National Science Foundation (NSF) and the U.S. Environmental Protection Agency (EPA) under NSF-EF0830117. Any opinions, findings, conclusions or recommendations expressed in this material are those of the authors do not necessarily reflect the views of the funding agencies. In addition, we appreciate the suggestions and comments given by the anonymous reviewers, editors and our group members Ya-nan Dong, Chen Wang.


## Appendix A. Supplementary data

Supplementary data associated with this article can be found, in the online version, at http://dx.doi.org/10.1016/j.colsurfa.2017.08.014.

## References


[1] T.J. Baker, C.R. Tyler, T.S. Galloway, Impacts of metal and metal oxide nanoparticles on marine organisms, Environ. Pollut. 186 (2014) 257–271.

[2] B. Faure, G. Salazar-Alvarez, A. Ahniyaz, I. Villaluenga, G. Berriozabal, Y.R. De Miguel, L. Bergström, Dispersion and surface functionalization of oxide nanoparticles for transparent photocatalytic and UV-protecting coatings and sunscreens, Sci. Technol. Adv. Mater. 14 (2013) 301–304.

[3] M. Farré, K. Gajda-Schrantz, L. Kantiani, D. Barceló, Ecotoxicity and analysis of nanomaterials in the aquatic environment, Anal. Bioanal. Chem. 393 (2009) 81–95.

[4] G.E. Batley, J.K. Kirby, M.J. McLaughlin, Fate and risks of nanomaterials in aquatic and terrestrial environments, Acc. Chem. Res. 46 (2012) 854–862.

[5] P. Westerhoff, B. Nowack, Searching for global descriptors of engineered nanomaterial fate and transport in the environment, Acc. Chem. Res. 46 (2012) 844–853.

[6] R. Kaegi, A. Voegelin, C. Ort, B. Sinnet, B. Thalmann, J. Krismer, H. Hagendorfer, M. Elumelu, E. Mueller, Fate and transformation of silver nanoparticles in urban wastewater systems, Water Res. 47 (2013) 3866–3877.

[7] K.L. Garner, A.A. Keller, Emerging patterns for engineered nanomaterials in the environment: a review of fate and toxicity studies, J. Nanopart. Res. 16 (2014) 1–28.

[8] M. Zhu, H. Wang, A.A. Keller, T. Wang, F. Li, The effect of humic acid on the aggregation of titanium dioxide nanoparticles under different pH and ionic strengths, Sci. Total Environ. 487 (2014) 375–380.

[9] S.M. Louie, R.D. Tilton, G.V. Lowry, Effects of molecular weight distribution and chemical properties of natural organic matter on gold nanoparticle aggregation, Environ. Sci. Technol. 47 (2013) 4245–4254.

[10] K.L. Chen, M. Elimelech, Aggregation and deposition kinetics of fullerene (C60) nanoparticles, Langmuir 22 (2006) 10994–11001.

[11] L.E. Barton, M. Therezien, M. Auffan, J.-Y. Bottero, M.R. Wiesner, Theory and methodology for determining nanoparticle affinity for heteroaggregation in environmental matrices using batch measurements, Environ. Eng. Sci. 31 (2014) 421–427.

[12] J.T. Quik, I. Velzeboer, M. Wouterse, A.A. Koelmans, D. van de Meent, Heteroaggregation and sedimentation rates for nanomaterials in natural waters, Water Res. 48 (2014) 269–279.

[13] Y. Peng, L.C. Kai, Release kinetics of multiwalled carbon nanotubes deposited on silica surfaces: QCM-D measurements and modeling, Environ. Sci. Technol. 48 (2014) 4406.

[14] K.A. Huynh, J.M. McCaffery, K.L. Chen, Heteroaggregation of multiwalled carbon nanotubes and hematite nanoparticles: rates and mechanisms, Environ. Sci. Technol. 46 (2012) 5912–5920.

[15] T. Tong, K. Fang, S.A. Thomas, J.J. Kelly, K.A. Gray, J.F. Gaillard, Chemical

interactions between nano-ZnO and Nano-$TiO_2$ in a natural aqueous medium, Environ. Sci. Technol. 48 (2014) 7924–7932.
[16] X. Qu, P. Alvarez, Q. Li, Applications of nanotechnology in water and wastewater treatment, Water Res. 47 (2013) 3931–3946.
[17] S. Sarkar, E. Guibal, F. Quignard, A. Sengupta, Polymer-supported metals and metal oxide nanoparticles: synthesis, characterization, and applications, J. Nanopart. Res. 14 (2012) 1–24.
[18] S. Aula, S. Lakkireddy, K. Jamil, A. Kapley, A.V.N. Swamy, H.R. Lakkireddy, Biophysical, biopharmaceutical and toxicological significance of biomedical nanoparticles, RSC Adv. 5 (2015) 47830–47859.
[19] M. Sailor, J. Park, Hybrid nanoparticles for detection and treatment of cancer, Adv. Mater. 24 (2012) 3779–3802.
[20] R. Upadhyay, M. Tripathi, P. Chawla, A. Pandey, Performance of $CeO_2$–$TiO_2$-admixed photoelectrode for natural dye-sensitized solar cell, J. Solid State Electrochem. 18 (2014) 1889–1892.
[21] K. Milenova, K. Zaharieva, Z. Cherkezova-Zheleva, B. Kunev, V. Blaskov, I. Stambolova, I. Mitov, Photodiscoloration of reactive black 5 dye using mechanochemically activated $TiO_2$–$CeO_2$ photocatalysts, Mater. Methods Technol. 8 (2014) 241–249.
[22] A. Bhosale, S. Kulal, V. Gurame, P. Patil, Spray deposited $CeO_2$–$TiO_2$ counter electrode for electrochromic devices, Bull. Mater. Sci. 38 (2015) 483–491.
[23] S. Wang, Q. Yang, Z. Bai, S. Wang, H. Chen, Y. Cao, Catalytic wet air oxidation of wastewater of the herbicide fomesafen production with $CeO_2$-$TiO_2$ catalysts, Environ. Eng. Sci. 32 (2015) 389–396.
[24] C. Karunakaran, P. Navamani, P. Gomathisankar, Particulate sol–gel synthesis and optical and electrical properties of $CeO_2$/$TiO_2$ nanocomposite, J. Iran. Chem. Soc. 12 (2015) 75–80.
[25] M. Farré, J. Sanchís, D. Barceló, Analysis and assessment of the occurrence, the fate and the behavior of nanomaterials in the environment TrAC, Trends Anal. Chem. 30 (2011) 517–527.
[26] H. Wang, Y.N. Dong, M. Zhu, X. Li, A.A. Keller, T. Wang, F. Li, Heteroaggregation of engineered nanoparticles and kaolin clays in aqueous environments, Water Res. 80 (2015) 130–138.
[27] P.D. Yates, G.V. Franks, S. Biggs, G.J. Jameson, Heteroaggregation with nanoparticles: effect of particle size ratio on optimum particle dose, Colloids Surf. A 255 (2005) 85–90.
[28] P. Dusak, A. Mertelj, S. Kralj, D. Makovec, Controlled heteroaggregation of two types of nanoparticles in an aqueous suspension, J. Colloid Interface Sci. 438 (2015) 235–243.
[29] A. Praetorius, J. Labille, M. Scheringer, A. Thill, K. Hungerbuhler, J.Y. Bottero, Heteroaggregation of titanium dioxide nanoparticles with model natural colloids under environmentally relevant conditions, Environ. Sci. Technol. 48 (2014) 10690–10698.
[30] Carrentero, A.,Villepin, R., Brunel, L., Carries, J., Turbiscan LAb User Guide, Formulaction, France (2005).
[31] J. Santos, N. Calero, J. Munoz, Optimization of a green emulsion stability by tuning homogenization rate, RSC Adv. 6 (2016) 57563–57568.
[32] M.S. Álvarez Cerimedo, C.H. Iriart, R.J. Candal, M.L. Herrera, Stability of emulsions formulated with high concentrations of sodium caseinate and trehalose, Food Res. Int. 43 (2010) 1482–1493.
[33] B. Xu, W. Kang, L. Meng, R. Yang, S. Liu, L. Zhang, Synthesis, aggregation behavior and emulsification characteristic of a multi-sticker amphiphilic polymer, J. Macromol. Sci. Part A 50 (2013) 302–309.
[34] L. Zhao, S. Zhang, H. Uluko, L. Liu, J. Lu, H. Xue, F. Kong, J. Lv, Effect of ultrasound pretreatment on rennet-induced coagulation properties of goat's milk, Food Chem. 165 (2014) 167–174.
[35] M. Wiśniewska, K. Terpiłowski, S. Chibowski, E. Chibowski, T. Urban, Studies of the alumina suspension stability in the presence of anionic polymer—influences of polymer molecular weight, its concentration and solution pH, Mol. Cryst. Liq. Cryst. 555 (2012) 7–16.
[36] M. Wiśniewska, K. Terpiłowski, S. Chibowski, T. Urban, V.I. Zarko, V.M. Gun'ko, Effect of polyacrylic acid (PAA) adsorption on stability of mixed alumina-silica oxide suspension, Powder Technol. 233 (2013) 190–200.
[37] L. Zhao, S. Zhang, H. Uluko, L. Liu, J. Lu, H. Xue, F. Kong, J. Lv, Effect of ultrasound pretreatment on rennet-induced coagulation properties of goat's milk, Food Chem. 165 (2014) 167–174.
[38] M. Wiśniewska, K. Terpiłowski, S. Chibowski, E. Chibowski, T. Urban, SStudies of the Alumina Suspension Stability in the Presence of Anionic Polymer—Influences of Polymer Molecular Weight, its Concentration and Solution pH, Mol. Cryst. Liq. Cryst. 555 (2012) 7–16.
[39] M. Wiśniewska, K. Terpiłowski, S. Chibowski, T. Urban, V.I. Zarko, V.M. Gun'ko, Effect of polyacrylic acid (PAA) adsorption on stability of mixed alumina-silica oxide suspension, Powder Technol. 233 (2013) 190–200.
[40] J.R. Conway, A.S. Adeleye, J. Gardeatorresdey, A.A. Keller, Aggregation dissolution, and transformation of copper nanoparticles in natural waters, Environ. Sci. Technol. 49 (2015) 2749–2756.
[41] Y. Han, D. Kim, G. Hwang, B. Lee, I. Eom, P.J. Kim, M. Tong, H. Kim, Aggregation and dissolution of ZnO nanoparticles synthesized by different methods: influence of ionic strength and humic acid, Colloids Surf. A 451 (2014) 7–15.
[42] X. Liu, J.R. Ray, C.W. Neil, Q. Li, Y.S. Jun, Enhanced colloidal stability of $CeO_2$ nanoparticles by ferrous ions: adsorption, redox reaction, and surface precipitation, Environ. Sci. Technol. 49 (2015) 5476–5483.
[43] F. Piccapietra, L. Sigg, R. Behra, Colloidal stability of carbonate-coated silver nanoparticles in synthetic and natural freshwater, Environ. Sci. Technol. 46 (2012) 818–825.
[44] M. Tejamaya, I. Römer, R.C. Merrifield, J.R. Lead, Stability of citrate PVP, and PEG coated silver nanoparticles in ecotoxicology media, Environ. Sci. Technol. 46 (2012) 7011.
[45] K.A. Huynh, J.M. Mccaffery, K.L. Chen, Heteroaggregation of multiwalled carbon nanotubes and hematite nanoparticles: rates and mechanisms, Environ. Sci. Technol. 46 (2012) 5912–5920.
[46] F.M. Omar, H.A. Aziz, S. Stoll, Aggregation and disaggregation of ZnO nanoparticles: influence of pH and adsorption of Suwannee River humic acid, Sci. Total Environ. 468–469 (2014) 195–201.
[47] H. Wang, Y.N. Dong, M. Zhu, X. Li, A.A. Keller, T. Wang, F. Li, Heteroaggregation of engineered nanoparticles and kaolin clays in aqueous environments, Water Res. 80 (2015) 130–138.
[48] D. Zhou, A.I. Abdel-Fattah, A.A. Keller, Clay particles destabilize engineered nanoparticles in aqueous environments, Environ. Sci. Technol. 46 (2012) 7520–7526.
[49] A.A. Keller, H. Wang, D. Zhou, H.S. Lenihan, G. Cherr, B.J. Cardinale, R. Miller, Z. Ji, Stability and aggregation of metal oxide nanoparticles in natural aqueous matrices, Environ. Sci. Technol. 44 (2010) 1962–1967.
[50] H. Wang, A.S. Adeleye, Y. Huang, F. Li, A.A. Keller, Heteroaggregation of nanoparticles with biocolloids and geocolloids, Adv. Colloid Interface 226 (2015) 24–36.
[51] K. Li, Y. Chen, Effect of natural organic matter on the aggregation kinetics of $CeO_2$ nanoparticles in KCl and $CaCl_2$ solutions: measurements and modeling, J. Hazard. Mater. 209 (2012) 264–270.
[52] M. Luo, Y. Huang, M. Zhu, Y. Tang, T. Ren, J. Ren, H. Wang, F. Li, Properties of different natural organic matter influence the adsorption and aggregation behavior of $TiO_2$ nanoparticles, J. Saudi Chem. Soc. (2016).
[53] V.L. Pallem, H.A. Stretz, M.J.M. Wells, Evaluating aggregation of gold nanoparticles and humic substances using fluorescence spectroscopy, Environ. Sci. technol. 43 (2009) 7531–7535.
[54] X. Chai, G. Liu, X. Zhao, Y. Hao, Y. Zhao, Fluorescence excitation-emission matrix combined with regional integration analysis to characterize the composition and transformation of humic and fulvic acids from landfill at different stabilization stages, Waste Manage. 32 (2012) 438–447.
[55] W. Chen, P. Westerhoff, J.A. Leenheer, K. Booksh, Fluorescence excitation-emission matrix regional integration to quantify spectra for dissolved organic matter, Environ. Sci. Technol. 37 (2003) 5701–5710.
[56] J. Qi, Y.Y. Ye, J.J. Wu, H.T. Wang, F.T. Li, Dispersion and stability of titanium dioxide nanoparticles in aqueous suspension: effects of ultrasonication and concentration, Water Sci. Technol. 67 (2013) 147–151.
[57] H. Zhang, J.A. Smith, V. Oyanedel-Craver, The effect of natural water conditions on the anti-bacterial performance and stability of silver nanoparticles capped with different polymers, Water Res. 46 (2012) 691–699.
[58] H. Wang, J. Qi, A.A. Keller, M. Zhu, F. Li, Effects of pH, ionic strength and humic acid on the removal of $TiO_2$ nanoparticles from aqueous phase by coagulation, Colloids Surf. A 450 (2014) 161–165.
[59] I. Chowdhury, N.D. Mansukhani, L.M. Guiney, M.C. Hersam, D. Bouchard, Aggregation and stability of reduced graphene oxide: complex roles of divalent cations, pH, and natural organic matter, Environ. Sci. Technol. 49 (2015) 10886–10893.
[60] J. Liu, X.F. Huang, L.J. Lu, M.X. Li, J.C. Xu, H.P. Deng, Turbiscan lab expert analysis of the biological demulsification of a water-in-oil emulsion by two biodemulsifiers, J. Hazard. Mater. 190 (2011) 214–221.
[61] F. Loosli, P. Le Coustumer, S. Stoll, $TiO_2$ nanoparticles aggregation and disaggregation in presence of alginate and Suwannee River humic acids. pH and concentration effects on nanoparticle stability, Water Res. 47 (2013) 6052–6063.
[62] W. Lin, M. Kobayashi, M. Skarba, C. Mu, P. Galletto, M. Borkovec, Heteroaggregation in binary mixtures of oppositely charged colloidal particles, Langmuir 22 (2006) 1038–1047.
[63] Y. Zhang, Y. Chen, P. Westerhoff, J. Crittenden, Impact of natural organic matter and divalent cations on the stability of aqueous nanoparticles, Water Res. 43 (2009) 4249–4257.
[64] J. Gregory, Rates of flocculation of latex particles by cationic polymers, J. Colloid Interface Sci. 42 (1973) 448–456.
[65] C. Shen, L. Wu, S. Zhang, H. Ye, B. Li, Y. Huang, Heteroaggregation of microparticles with nanoparticles changes the chemical reversibility of the microparticles' attachment to planar surfaces, J. Colloid Interface Sci. 421 (2014) 103–113.
[66] J.Q. Jiang, N. Graham, C. André, G.H. Kelsall, N. Brandon, Laboratory study of electro-coagulation–flotation for water treatment, Water Res. 36 (2002) 4064–4078.
[67] N.C. Birben, C.S. Uyguner-Demirel, S. Sen-Kavurmaci, Y.Y. Gurkan, N. Turkten, Z. Cinar, M. Bekbolet, Comparative evaluation of anion doped photocatalysts on the mineralization and decolorization of natural organic matter, Catal. Today 240 (2015) 125–131.
[68] Z. Wang, Z. Wu, S. Tang, Characterization of dissolved organic matter in a submerged membrane bioreactor by using three-dimensional excitation and emission matrix fluorescence spectroscopy, Water Res. 43 (2009) 1533–1540.
[69] Y. Adachi, L. Feng, M. Kobayashi, Kinetics of flocculation of polystyrene latex particles in the mixing flow induced with high charge density polycation near the isoelectric point, Colloids Surf. A 471 (2015) 38–44.
[70] M. Erhayem, M. Sohn, Effect of humic acid source on humic acid adsorption onto titanium dioxide nanoparticles, Sci. Total Environ. 470–471 (2014) 92–98.
[71] B. Pan, D. Zhang, H. Li, M. Wu, Z. Wang, B. Xing, Increased adsorption of sulfamethoxazole on suspended carbon nanotubes by dissolved humic acid, Environ. Sci. Technol. 47 (2013) 7722–7728.
[72] R.A. Ruehrwein, D.W. Ward, Mechanism of clay aggregation by polyelectrolytes, Soil Sci. 73 (1952) 485–492.
[73] J.T. Quik, I. Lynch, K. Van Hoecke, C.J. Miermans, K.A. De Schamphelaere,

C.R. Janssen, K.A. Dawson, M.A.C. Stuart, D. Van De Meent, Effect of natural organic matter on cerium dioxide nanoparticles settling in model fresh water, Chemosphere 81 (2010) 711–715.

[74] P.D. Yates, G.V. Franks, G.J. Jameson, Orthokinetic heteroaggregation with nanoparticles: effect of particle size ratio on aggregate properties, Colloids Surf. A 326 (2008) 83–91.

[75] A.A. Markus, J.R. Parsons, E.W. Roex, P. de Voogt, R.W. Laane, Modeling aggregation and sedimentation of nanoparticles in the aquatic environment, Sci. Total Environ. 506–507 (2015) 323–329.

[76] T. Tong, K. Fang, Sara A. Thomas, John J. Kelly, Kimberly A. Gray, Jean-Francois Gaillard, Chemical interactions between nano-ZnO and nano-$TiO_2$ in a natural aqueous medium, Environ. Sci. Technol. (2014) 7924–7936.